AD-A042 491 AIR FORCE GEOPHYSICS LAB HANSCOM AFB MASS F/G 4/1
EXCEDE II.(U)
DEC 76 R R O'NEIL, E T LEE, A T STAIR
UNCLASSIFIED AFGL-TR-76-0308 NL

| OF |
AD A042 491

END
DATE FILMED
8-77
DDC

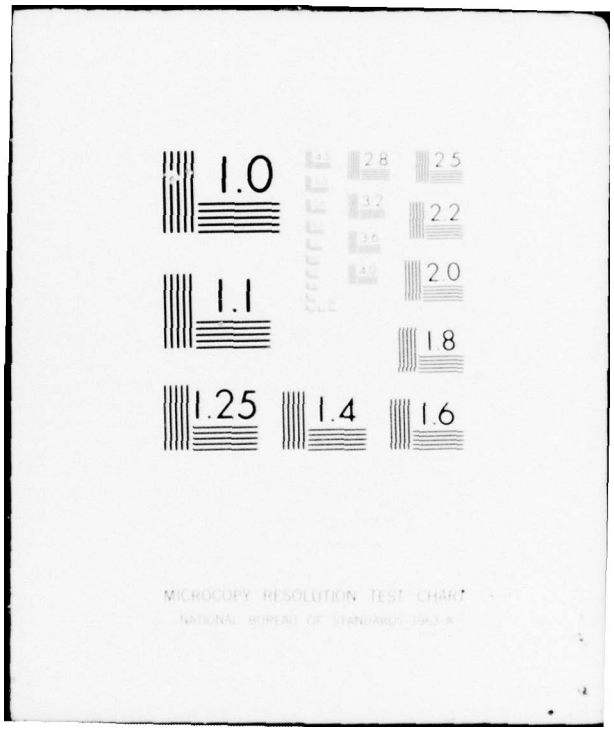
1.0
1.1
1.25
1.4
1.6
2.8
2.5
3.2
2.2
3.6
2.0
4.0
1.8
MICROCOPY RESOLUTION TEST CHART
NATIONAL BUREAU OF STANDARDS 1963 A

AFGL-TR-76-0308
ENVIRONMENTAL RESEARCH PAPERS, NO. 586

12

EXCEDE II

ROBERT R. O'NEIL
EDWARD T.P. LEE
A.T. STAIR, Jr.
JAMES C. ULWICK

21 December 1976

This research was sponsored in part by the Defense Nuclear Agency, Subtask L25AAXHX632, entitled "IR Phenomenology and Optical Code Data Base."

OPTICAL PHYSICS DIVISION PROJECT 2310
AIR FORCE GEOPHYSICS LABORATORY
HANSCOM AFB, MASSACHUSETTS 01731

AIR FORCE SYSTEMS COMMAND, USAF

This report has been reviewed by the ESD Information Office (OI) and is releasable to the National Technical Information Service (NTIS).

This technical report has been reviewed and is approved for publication.

FOR THE COMMANDER

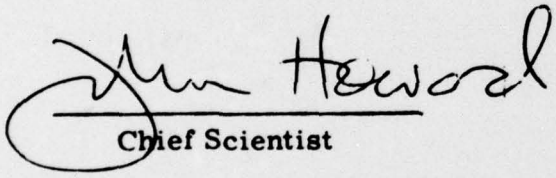

Chief Scientist

Qualified requestors may obtain additional copies from the Defense Documentation Center. All others should apply to the National Technical Information Service.

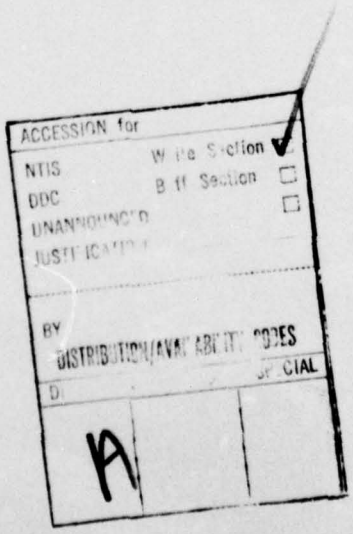

Unclassified

SECURITY CLASSIFICATION OF THIS PAGE (When Data Entered)

REPORT DOCUMENTATION PAGE

READ INSTRUCTIONS BEFORE COMPLETING FORM

1. REPORT NUMBER: AFGL-TR-76-0308	2. GOVT ACCESSION NO. AFGL-ERP-586
3. RECIPIENT'S CATALOG NUMBER	
4. TITLE (and Subtitle): EXCEDE II.	5. TYPE OF REPORT & PERIOD COVERED: Scientific. Interim.
6. PERFORMING ORG. REPORT NUMBER: ERP, No. 586	
7. AUTHOR(s): Robert R. O'Neil, James C. Ulwick, Edward T. P. Lee, A. T. Stair, Jr.	8. CONTRACT OR GRANT NUMBER(s): 17 G4
9. PERFORMING ORGANIZATION NAME AND ADDRESS: Air Force Geophysics Laboratory (OPR), Hanscom AFB, Massachusetts 01731	10. PROGRAM ELEMENT, PROJECT, TASK AREA & WORK UNIT NUMBERS: 2310G402, 61102F
11. CONTROLLING OFFICE NAME AND ADDRESS: Air Force Geophysics Laboratory (OPR), Hanscom AFB, Massachusetts 01731	12. REPORT DATE: 21 December 1976
	13. NUMBER OF PAGES: 38
14. MONITORING AGENCY NAME & ADDRESS (if different from Controlling Office): 12 38p.	15. SECURITY CLASS. (of this report): Unclassified
	15a. DECLASSIFICATION/DOWNGRADING SCHEDULE

16. DISTRIBUTION STATEMENT (of this Report)

Approved for public release; distribution unlimited.

17. DISTRIBUTION STATEMENT (of the abstract entered in Block 20, if different from Report)

9 Environmental research papers

18. SUPPLEMENTARY NOTES

This research was sponsored in part by the Defense Nuclear Agency, Subtask L25AAXHX632, entitled "IR Phenomenology and Optical Code Data Base."

19. KEY WORDS (Continue on reverse side if necessary and identify by block number)

Artificial aurora
Rocketborne electron accelerator
Infrared atmospheric emissions

20. ABSTRACT (Continue on reverse side if necessary and identify by block number)

EXCEDE is a program designed to study atmospheric infrared emissive processes induced by a rocketborne electron accelerator in the altitude range 80 to 140 km. The primary scientific interest is the investigation of the detailed production and loss processes of various excited electronic and vibrational states resulting in optical and infrared emission as energetic primary electrons and their secondary and all subsequent generation electrons are stopped in the atmosphere. The electron-induced optical and

→ next page

DD FORM 1 JAN 73 1473 EDITION OF 1 NOV 65 IS OBSOLETE

Unclassified

SECURITY CLASSIFICATION OF THIS PAGE (When Data Entered)

409578

/B

cont → infrared emissions simulate natural auroral processes with the very significant advantage that the dosing conditions of electron energy and power, deposition volume and altitude, and dosing duration are parameters that may be controlled and monitored. To date, three payloads have been launched in the EXCEDE series of artificial auroral experiments. The program status is reviewed and a follow on experiment, EXCEDE II, is described. Both rocket-based and ground-based imaging and spectroradiometric instruments are proposed. The feasibility of the scientific approach, the magnitude of the atmospheric emissions, the capabilities of ground-support systems, and the engineering design of the proposed experiment are extensions of the technology base established in the earlier EXCEDE launches.

Preface

The EXCEDE II experiment described in this report has evolved from the earlier launches in the program which involved numerous participants representing various agencies and contractors. Significant contributions to the experimental approach were made by E. McKenna, R. Narcisi, D. Newell, E.R. Huppi, J. Sandock, and J. LaSpina of AFGL, E. Allen of Space Data Corp., J.W. Carpenter, W. Reidy, and O. Shepherd of Visidyne, Inc., F. Bien and M. Camac of Aerodyne, Inc., D. Burt, K. Baker, D. Baker, G. Frodsham, and J. Kemp of Utah State University, D. Hansen and M. Schuler of HSS, Inc., W. Boquist and J. Fitzgerald of TIC, Inc., T. Neil Davis, Jr., N. Brown, and T. Hallinan of the University of Alaska, I.L. Kofsky of Photometrics, Inc., H. Mitchell of R and D Associates and H.C. Fitz, Jr. and Lieutenant Commander C. Thomas of DNA. The efficiency and assistance of Ms. Gloria Foss in the preparation of this report is gratefully acknowledged.

Contents

Illustrations

Tables

Excede II

I. INTRODUCTION

EXCEDE is a DNA/AFGL program designed to study auroral infrared emissive processes using a rocketborne electron accelerator operating in the altitude range 80 to 140 km. The concept of using a rocketborne electron accelerator in an artificial auroral experiment was initially proposed by Dr. A. T. Stair, Jr., of AFGL, in 1971. The primary scientific interest is the investigation of the detailed production and loss processes of various excited electronic and vibrational states resulting in optical and infrared emission as energetic primary electrons and their secondary and all subsequent generation electrons are stopped in the atmosphere. In the proposed artificial auroral experiment, the dosing conditions of: electron energy and power, deposition volume, deposition altitude, and dosing duration are parameters that may be controlled and monitored. In natural aurora, these excitation conditions must be inferred and the observed atmospheric emissions typically are effects integrated over a range of conditions (electron energy, electron-flux density, altitude, and dosing time). Observations of these integral effects make interpretation of optical/infrared emissions in terms of

(Received for publication 20 December 1976)

basic production and loss processes exceedingly complex. At present, considerable uncertainty exists in the interpretation of auroral optical and infrared emissions including such a well-studied feature as the auroral green line, $O(^1S)$ 5577 Å emission.[1-5]

2. PROGRAM STATUS

To date, three payloads have been launched in the EXCEDE series of artificial auroral experiments. The present document briefly reviews the program status and describes a proposed follow-on experiment. The initial three launches in the EXCEDE program are summarized in Table 1. The feasibility of the concept has been demonstrated by two engineering test launches designated PRECEDE (3 kV, 1A) launched on 17 October 1974 from White Sands Missile Range, N.M. and EXCEDE II Test (3 kV, 10 A) launched from Poker Flat, Alaska on 13 April 1975. An experiment (EXCEDE SWIR) including photometers, liquid-nitrogen cooled radiometers, and an ion-mass spectrometer as rocket-based diagnostic instruments has been successfully flown at Poker Flat, Alaska on 28 February 1976 to determine principal production mechanisms, reaction rates, and infrared photon yields for NO and NO^+ infrared chemiluminescent processes. The detailed experimental approach in the EXCEDE: SWIR launch is presented by O'Neil et al., 1973.[6]

1. Rees, M.H. and Jones, R.A. (1973) Time dependent studies of the aurora—II. Spectroscopic morphology, Planet. Space Sci. 21:1213.
2. Judge, R.J. R. (1972) Electron excitation and auroral emission parameters, Planet. Space Sci. 20:2081.
3. Banks, P.M., Chappel, E.R., and Nagy, A.F. (1974) A new model for interaction of auroral electrons with the atmosphere: Spectral degradation, backscatter, optical emission, and ionization, J. Geophys. Res. 79 (No. 10):1459.
4. Rees, M.H. and Luckey, D. (1974) Auroral electron energy derived from ratio of spectroscopic emissions: 1. Model computations, J. Geophys. Res. 79 (No. 34):5181.
5. Slanger, T.G. and Black, G. (1973) $O(^1S)$ quenching profile between 75 and 115 km, Planet. Space Sci. 21:1757.
6. O'Neil, R.R., Lee, E.T.P., Huppi, E.R., and Stair, A.T., Jr. (1973) Project EXCEDE: SWIR Experiment, AFCRL-TR-73-0152, Environmental Research Papers, No. 437.

Table 1. Project EXCEDE: Status

Event	Launch	Nominal Power	Experiment Altitude Range	Summarized Results
PRECEDE	17 Oct 1974 WSMR*	2 kW (2.5 kV, 0.8 A)	80 to 120 km	Measured small vehicle potentials, excellent ground based optical measurements
EXCEDE II Test	13 Apr 1975 PFRR**	30 kW (3 kV, 10 A)	110 to 137 km	Rocket based photometric and radiometric data and ground based optical support
EXCEDE: SWIR	28 Feb 1976 PFRR**	3 kW (3 kV, 1 A)	80 to 99 km	Heavily instrumented payload and the optical ground support systems realized good data

*WSMR, White Sands Missile Range, New Mexico.

**PFRR, Poker Flat Rocket Range, Alaska.

3. PRECEDE

The initial launch in the EXCEDE program, designated PRECEDE, was a Nike Hydac Rocket (EX 407.41-1) instrumented with a 2-kW (2.5 kV, 0.8 A) electron accelerator launched at 10:20:00 UT on 17 October 1974 from White Sands Missile Range. This flight was an engineering test of the electron accelerator to be subsequently used on the heavily instrumented EXCEDE:SWIR experiment. The electron source, square-wave modulated at 0.5 Hz, was initiated at 95 km on payload ascent and continued through apogee (120 km) to a descent altitude of approximately 80 km, operating for an interval of 180 sec. The payload was launched from north to south so that the electron beam was deposited along the geomagnetic field above the payload (Figures 1 and 2). The trajectory for the PRECEDE launch was in the plane of the magnetic declination, 12° east, and the Tiff optical station was located to observe the payload along the magnetic field at approximately 110 km during payload descent. In this configuration the electron deposition volume, constrained along the magnetic field, presents a minimal source size for the photometric and spectrographic instruments located at the Tiff optical station. The Denver and Cloudcroft

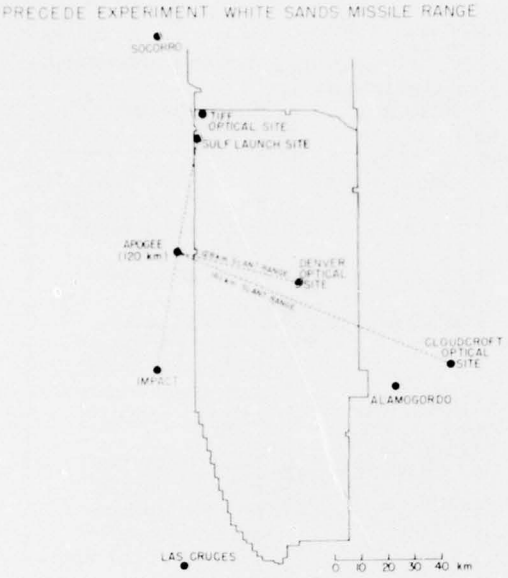

Figure 1. White Sands Missile Range, New Mexico, Indicating the Trajectory of the PRECEDE Launch and the Location of Three Optical Ground Stations

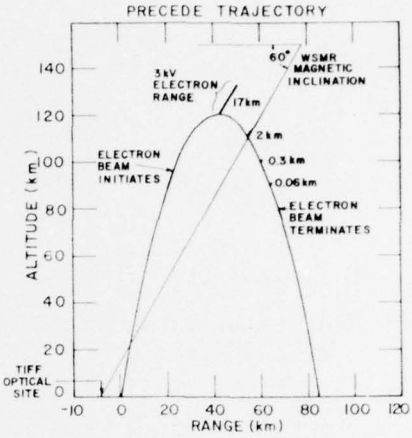

Figure 2. Flight Profile of the PRECEDE Launch Indicating the Calculated Practical Range of 3 kV Electrons Along the Magnetic Field and the Viewing Aspect of the Image Intensified Spectrograph and the Two-Color Telephotometer Located at the Tiff Optical Site

stations contained various camera systems to record the electron-induced atmospheric luminescence with viewing aspects arranged to image radiance along the magnetic field and record the size of electron-excited atmosphere. On board measurements included monitors of electron-beam voltage and current and a retarding potential analyzer to determine particle flux and vehicle potential.

Figure 3, a montage of PRECEDE photographs from Denver optical site (see Figure 1), is an illustration of the overall dimensions of the electron beam as a function of altitude. In Figure 4 is given in greater spatial detail: the electron-beam energy deposited above the payload along the magnetic field, the relatively faint electron-beam luminescence below the payload due to back-scattered electrons, and a bright chemiluminescent wake tangential to the payload trajectory due to rocket propellants (aluminum or aluminum compounds) reacting with atmospheric atomic oxygen. Figure 4, provided by the Cloudcroft optical station, was taken with an image orthicon system and represents an integration of several seconds. All three optical ground stations used radar controlled instrument mounts which located and tracked the payload within 1-arc min for the duration of the experiment. The precise tracking of the optical mounts

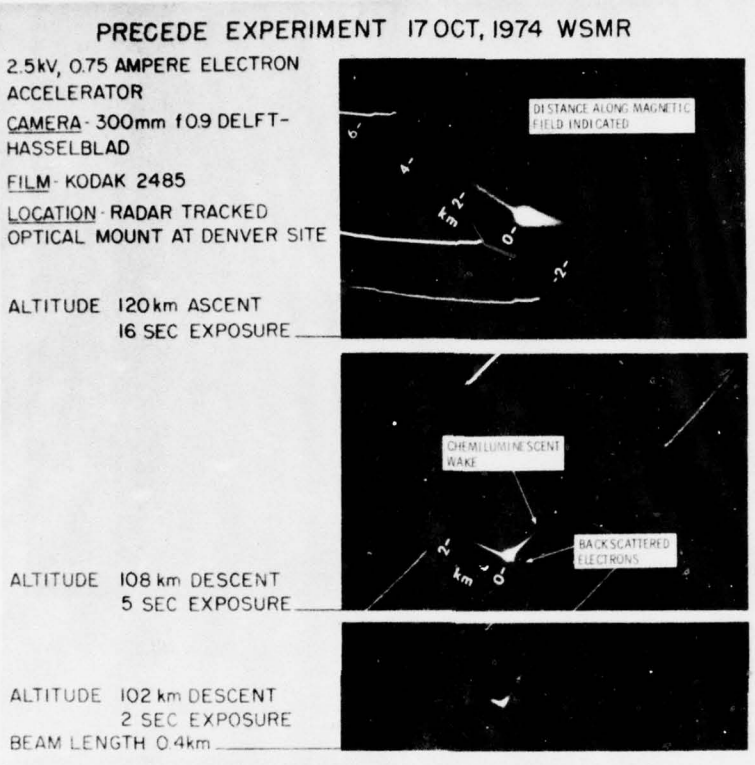

FIGURE 3. Photographs taken by TIC, Inc. of Bedford, Mass. from the Denver optical site.

Figure 3. Photographs Taken by TIC, Inc. of Bedford, Mass., from the Denver Optical Site

allowed the ground-based imaging systems, an image intensified spectrograph and the television and film cameras, to effectively utilize exposure times as long as 20 sec. For the spatial resolution of the imaging systems and the tracking precision of the optical mounts, effective exposure times were determined by the shutter-open period rather than by the focal-plane image smear.

The PRECEDE launch trajectory was configured such that the electron beam, originating from the nose of the payload, was deposited above the vehicle along the magnetic field without the use of an attitude control system. The nominal pitch angle ranged from 15 to 35 deg during the experiment and was 25 deg for the case represented in Figure 4. The dimensions of electron range and radial scatter indicated in Figure 3 and 4 are in good agreement with

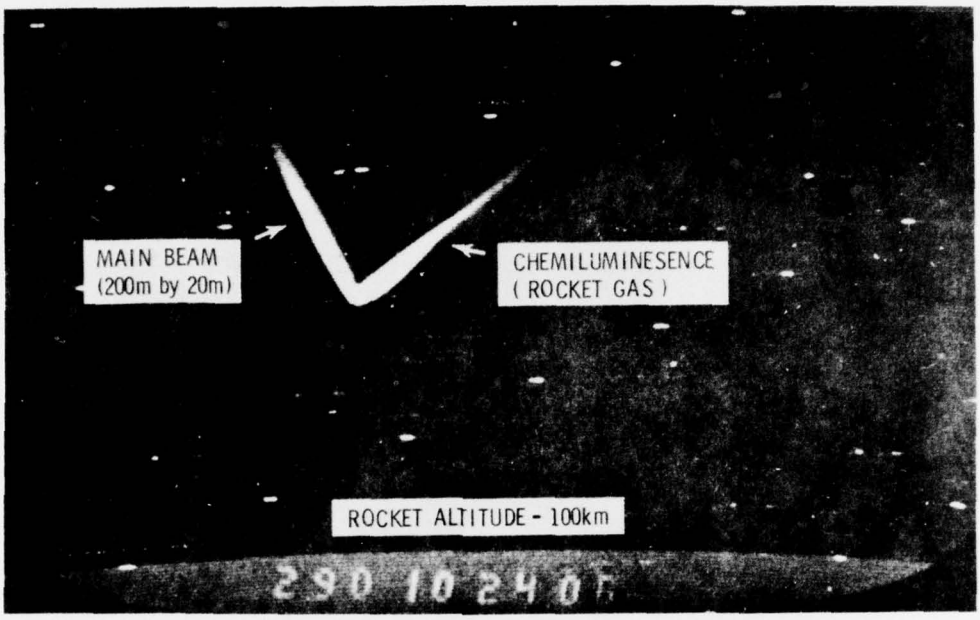

Figure 4. Atmospheric Emission Induced by the PRECEDE Launch as Recorded by an Image Orthicon at the Cloudcroft Optical Site

the calculations of Berger et al.,[7,8] which were initiated in support of the rocket-borne electron-accelerator experiment of Hess et al.[9]

4. EXCEDE II TEST

The second launch in the EXCEDE program consisted of a Castor rocket (C75-1) instrumented with two 3-kV electron accelerators, photometers, IR radiometers, instruments to measure particle flux and vehicle potential, and L-band, P-band, and S-band transmitters launched from Poker Flat Research Range

7. Berger, M.J., Seltzer, S.M., and Maeda, K. (1970) Energy deposition by auroral electrons in the atmosphere, J. Atmos. and Terr. Phys. 32 (No. 6):1015.

8. Berger, M.J., Seltzer, S.M., and Maeda, K. (1974) Some new results on electron transport in the atmosphere, J. Atmos. and Terr. Phys. 36:591.

9. Hess, W.N., Trichel, M.C., Davis, T.N., Beggs, W.C., Kraft, G.E., Stassinopoulos, E., and Maier, E.J.R. (1971) Artificial aurora experiment: Experiment and principal results, J. Geophys. Res. 76 (No. 25):6067.

at 09:46:00 UT on 13 April 1975 during a period of low auroral activity. The two electron accelerators inadvertently pulsed independently with a peak power output of 30 kW. The accelerators were activated at 100 km and operated through apogee (137 km) for a period of 100 sec. Ground-based instrumentation included a telephotometer measuring 3914 and 5577 Å emission and four low-light television systems situated at selected geographical positions with respect to the rocket trajectory. The optical ground stations manually tracked the artificial aurora with the television systems. Radio-frequency transmission measurements indicate electron density in the vicinity of the rocket was on the order of 10^8 electrons cm^{-3}. Peak radiance values measured by the coaligned rocketborne photometers and radiometers were 34 MR at 3914Å, 1.3 MR at 5577Å, 44 MR at 2.7 μm, and 3.4 MR at 4.3 μm. The payload design is given by Shepherd et al.[10]

5. EXCEDE: SWIR

The EXCEDE:SWIR rocketborne electron-accelerator experiment was successfully launched from Poker Flat, Alaska on 28 February 1976 at 05 hr: 46 min: 40 sec into a quiet night atmosphere. A Sergeant rocket engine (vehicle number EX 630.42-1) carried the 32-in. diameter 1700-lb payload to an apogee of 99 km. A 3-kW (3 kV, 1 A) electron beam was initiated at approximately 90 km on payload ascent, continued through apogee and survived to approximately 75 km on payload descent, providing a total experiment time of approximately 100 sec. Atmospheric emissions induced by the pulsed beam, square-wave modulated at 0.5 Hz, were readily recorded by rocket-based photometers and liquid-nitrogen cooled radiometers as well as by ground-based television and telephotometer instruments. With one minor exception, all payload instrumentation functioned as designed including: the pulsed electron accelerator, all 22 UV and visible photometers, 10 of 12 liquid-nitrogen cooled radiometer data channels (one dual-channel instrument failed prior to launch), and the positive ion-mass spectrometer. The ground-based systems, low-light television and dual-channel telephotometer, recorded excellent data. Preliminary results of this launch are summarized by O'Neil et al.[11]

---

10. Shepherd, O., Carpenter, J.W., Reidy, W.P., Sheehan, W.A., and Zehnpfeunig, T.F. (1975) The Design and Flight Test of a 30 kw Rocket-Borne Electron Accelerator Module (EXCEDE II Test) HAES Report No. 22, AFCRL-TR-75-0379.

11. O'Neil, R.R., Stair, A.T., Jr., Ulwick, J.C., Burt, D., and Narcisi, R. (1976) EXCEDE:SWIR experiment, Quick Look Data Report.

6. VEHICLE POTENTIAL

As part of the initial design study, a theoretical estimate[12] of the time-dependent vehicle potential indicated a steady state potential on the order of a few tens of volts positive for the experimental conditions applicable to the proposed PRECEDE launch. The time-dependent calculation shows an oscillatory vehicle potential of several hundred volts which converges to the small positive steady state potential within approximately 20 μsec. The discharge mechanism is the return to the vehicle skin of secondary electrons produced by ionization of the ambient atmosphere by the energetic primary beam. Measured steady state vehicle potentials increase with altitude as the beam-induced electron density decreases with atmospheric density. For the conditions of the PRECEDE launch, beam-induced electron densities on the order of 10^7 to 10^8 cm^{-3} were estimated at 105 km (O'Neil et al.[13]). The retarding potential analyzer results of the PRECEDE launch[14, 15] confirm the preflight steady state theoretical estimate of vehicle potential with a measured value of less than +120 V at 120 km and less than +17 V at 90 km. The EXCEDE II test flight indicates a vehicle potential of less than +200 V but is an upper limit value due to an instrument malfunction. In the EXCEDE:SWIR launch the positive-ion mass spectrometer of Dr. Narcisi of AFGL included a bias plate at the instrument sampling point maintained at a potential that was periodically stepped in the range of -30 to -260 V. Initial interpretation of the data indicates the vehicle potential of the electron emitting payload was typically less than 60 V positive, with a potential less than this magnitude for the major portion of the flight. It is noted that the vehicle potentials reported to date in the EXCEDE results are upper limit values rather than definitive measurements, due to the stepped nature of the sampling voltages and the measurement technique which includes the integral effects of secondary electron energy distributions.

---

12. Bien, F. and Baum, H.R. (1974) Detailed Investigation of Transient Electron Beam Deposition into the Atmosphere, Aerodyne Research, Inc., Report ARI-RR-50, Contract No. F19628-73-C-0048, Subcontract No. PO43081.

13. O'Neil, R.R., Huppi, E.R., and Lee, E.T.P. (1975) PRECEDE experiment: Ground based telephotometer measurements of N_2^+IN 3914Å and O(^{1}S) 5577Å emission (abstract), EOS Trans. AGU **56** (No. 12):1035.

14. Sandock, J.A., Burt, D.A. and Bien, F. (1975) PRECEDE experiment (abstract,) EOS Trans. AGU **56** (No. 12):1035.

15. Bien, F., Baum, H., and Tait, K. (1975) An analysis of transient vehicle charging in the EXCEDE experiment (abstract), EOS Trans. AGU, **56** (No. 12):1035.

Cambou et al.,[16] Cambou et al.,[17] and Reme et al.,[18] similarly report a positive vehicle potential small in comparison with the accelerator voltage in the joint Franco-Soviet rocketborne electron-accelerator experiments in project ARAKS (Artificial Radiation and Auroras between Kerguelen and the Soviet Union). Vehicle potential as measured by retarding potential analyzers on the January and February 1975 launches from Kerguelen Island was less than approximately 200 V at altitudes between 130 to 200 km with smaller vehicle potentials at lower altitudes, approximately +20 V at 100 km. These compare with primary electron energies of 27 and 15 kV and currents of 0.5 and 1.0 A, square-wave modulated with pulse periods of both 0.04 and 5.12 sec. The vehicle potentials measured in the EXCEDE and ARAKS experiments agree in general magnitude at similar altitudes and the effects of these relatively small positive potentials are inconsequential to the experimental concept as proposed for EXCEDE II.

7. EXCEDE II: EXPERIMENT CONCEPT

The major innovations in the proposed EXCEDE II experiment are a significant increase in the power of the rocketborne electron accelerator and the addition of optical- and infrared-spectral instruments to record detailed band profiles rather than photometric and radiometric instruments that isolate specific wavelength intervals as used in the earlier launches. The proposed nominal electron-accelerator power is 120 kW (3 kV, 40 A) using 4 electron-gun modules each providing a 10-A beam. The engineering design of the electron accelerator is an extension of the approach used in both the PRECEDE and EXCEDE:SWIR payloads as developed by Mr. David Burt of Utah State University. The proposed accelerators use tungsten filaments which are activated at approximately 95 km on payload ascent. As evidenced in the earlier payloads, the tungsten filaments

16. Cambou, F., Dokoukine, V.S., Ivchenko, V.N., Managadze, G.G., Migulin, V.V., Nazarenko, O.K., Nesmyanovitch, A.T., Pyatsi, A.KH., Sagdeev, R.Z., and Zhulin, I.A. (1975) The Zarmitza rocket experiment of electron injection, to be published in Space Research XV and Life Time Sciences XIII.

17. Cambou, F., Sagdeev, R.Z., Zhu'in, I.A., Charles, G., and Dokoukme, V.S. (1976) General description of the ARAKS experiments (abstract), Program and Abstracts for the Symposium on Active Experiments in Space Plasmas, COSPAR, URSI, and IAGA, June 3-5, 1976, Boulder, Colo.

18. Reme, H., Saint-Marc, A., Vigo, J.M., Gringauz, K.I., Managadze, G.C., Lyakhov, S.B., Smirnova, L.P., Schutte, N.M., and Sheldon, W.R. (1976) Results of the ARAKS particle experiments (abstract), Program and Abstracts for the Symposium on Active Experiments in Space Plasmas, COSPAR, URSI, and IAGA, June 3-5, 1976, Boulder, Colo.

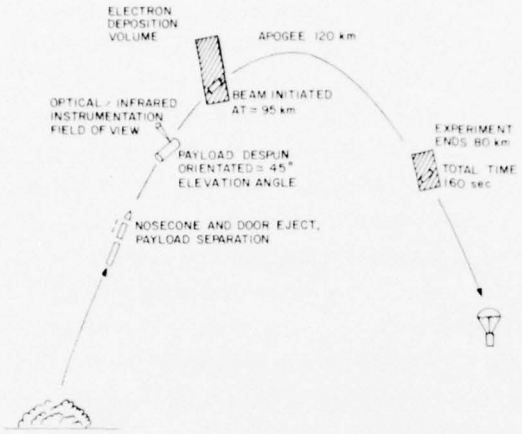

Figure 5. Flight Profile for the Proposed EXCEDE II Experiment

continue to provide an electron beam to descent altitudes of approximately 75 km, operating in the rarefied atmosphere of the payload wake during the descent trajectory.

The EXCEDE II flight profile is indicated in Figure 5. As indicated, the payload is despun and arranged such that the long dimension is in the plane of the trajectory and elevated at an angle of approximately 43 deg after nosecone and door ejection and payload separation. The electron accelerators initiate a pulse sequence at approximately 95 km on payload ascent which is continued through apogee, 120 km, and is anticipated to continue to approximately 80 km on payload descent providing a total experiment duration of 160 sec. At 75 km on descent the electron accelerators are separated from the diagnostic instrumentation which is recovered. The payload orientation during the experimental launch period is shown in Figure 6. In this position the electron accelerator and instruments are oriented such that:

(1) The electron-beam injection angle is canted 30 deg from the normal to the payload (Figure 6).

(2) The spectral instruments have a field of view normal to the payload, intersecting the magnetic field (and the electron-beam axis) at 30 deg, and arranged with respect to the vehicle velocity to observe both the prompt emissions in the primary electron deposition region and slower emissions in the electron-beam afterglow. In this configuration the following experimental conditions are satisfied:

(a) The optical/infrared spectral instruments have an essentially continuous look at the beam-induced emissions for several spectral scans from a given aspect with minimal apparent source variations due to the effects of spin modulation.

(b) The onboard infrared instruments operate at a field of view axis elevation angle of 47 deg (assuming launch from Poker Flat, Alaska), thus avoiding thermal radiation from the earth and lower atmosphere.

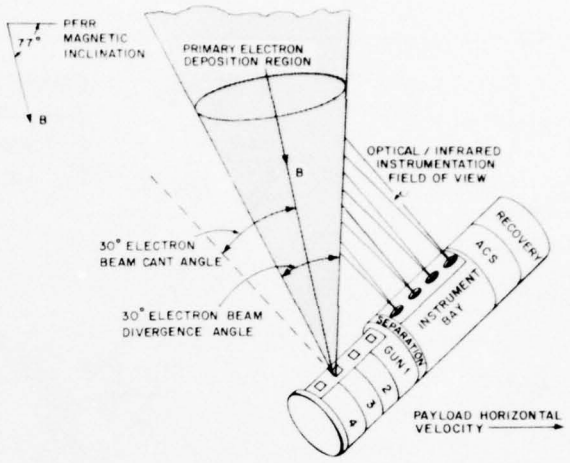

Figure 6. Payload Orientation for EXCEDE II with Only Electron Gun 3 Shown Operating. The attitude control system (ACS) maintains the indicated position in pitch, yaw, and roll for the duration of the experiment

The experimental approach is to turn the electron source on for several seconds in which the spectral instruments record one or more spectra. The payload-based instruments have full-cone fields of view, which are approximately 5 deg or less, and thus observe the primary electron deposition region as an extended source (see Figure 6). After beam turn-on the radiance of each emitting species, as observed by the payload based sensors, is determined in part by: the characteristic production and/or emission time constant of a given excited state, payload velocity, and the instrumentation viewing aspect. Since the horizontal component of payload velocity is anticipated to be on the order of several hundred meters per second, production and/or emission processes having characteristic times on the order of 0.001 sec or longer are anticipated to show an afterglow emission displacement that is significant in terms of the primary electron deposition volume near the payload. The afterglow emission effect is demonstrated in Figures 3 and 4 by the chemiluminescent rocket propellants tangential to the payload trajectory. As viewed from the payload instrument bay, the region near the vehicle contributes most of the apparent brightness since the electron energy deposited per unit volume varies as the square of reciprocal distance from the vehicle in the near field and the electron-beam luminescence overfills the optical system fields of view. In Figure 7, radiance as a function of integrated viewing depth along the optical axis is shown for N_2^+ 1N(0-0) 3914Å emission. The results in Figure 7 assume the conditions of Figure 6 and an electron source detector separation of 50 cm. In addition the electron beam has been considered to originate from a single cathode and to diverge with a uniform current density into a 30-deg full cone. The optical axis of sensor B in Figure 7

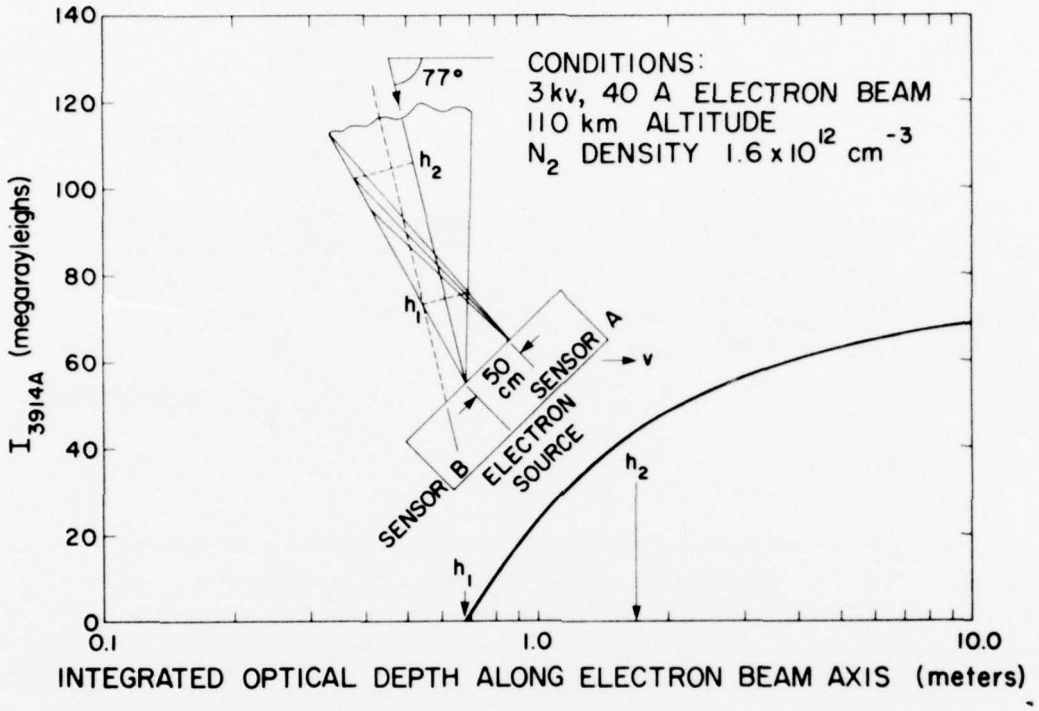

Figure 7. The Effective Radiance of Primary Electron Induced Emission with Distance from the Vehicle for Payload Based Sensors

is arranged parallel to the electron-beam axis providing an increased optical depth into the primary electron deposition goemetry. However, as configured in Figure 7, sensor A observes a radiance due to prompt emissions of 60 percent of sensor B with additional practical advantages in payload packaging and alignment tolerances inherent in the crossed electron-beam optical axis system. The orientation of sensor A also effectively observes the afterglow radiation of slower production/emission processes. As demonstrated in Figure 7, payload-based optical sensors effectively observe emissions only in the first few meters near the payload, with an absolute magnitude three orders of magnitude greater than a bright aurora (N_2^+ 3914Å emission is 50 kR in an IBC Class III aurora [19]).

19. Vallance-Jones, A. (1971) Auroral spectroscopy Space Sci. Reviews 11:776.

8. SHORT WAVE INFRARED CHEMISTRY

The optical/infrared instruments, as shown in Figure 6, integrate across a region where the energy density deposited by the primary electrons varies as the square of the reciprocal distance from the payload. For the conditions of Sensor A in Figure 7 the dosing magnitude ranges from 2.5×10^{12} to 1.5×10^{13} ion pairs $cm^{-3} sec^{-1}$ at 110 km in the bright core of the electron deposition volume. The time a given atmospheric volume element is irradiated by the electron beam is determined by the transit time of the electron cloud, approximately 2 to 5 msec for the optically observed region of Figure 7 assuming a down range payload velocity of 200 m sec^{-1}. Calculated time-dependent concentrations of the beam-induced electron density, major ion species and selected metastable states are shown in Figure 8. The reaction set of Table 2 has been used with the Kutta-Merson method to solve the coupled differential equations.[20] In Figure 8 is assumed an ion-pair production rate 10^{12} ion pairs $cm^{-3} sec^{-1}$ for 5×10^{-3} sec and initial atmospheric conditions as given by the Keneshea et al.[21] model atmosphere for a nighttime 30 deg northern latitude case for November 1970. Initial concentrations are $1.2 \times 10^{12} cm^{-3}$ for N_2, $2.2 \times 10^{11} cm^{-3}$ for O_2, and 8.6×10^{10} cm^{-3} for O with a kinetic temperature of 341°K. The initial NO concentration is assumed to be $10^7 cm^{-3}$. The results of Figure 8 indicate:

(a) N_2^+ concentration decays rapidly after the beam no longer irradiates a given volume element due to dissociative recombination and charge transfer. At 110 km dissociative recombination of N_2^+ is the dominant loss process at electron densities of $5 \times 10^8 cm^{-3}$ or greater; reactions with atomic oxygen dominate at lower electron densities.

(b) The concentration of NO^+ decreases after electron excitation ceases due to rapid dissociative recombination at high electron densities until approximately 0.1 sec, when the electron density has decreased by an order of magnitude. From 0.1 to 1 sec, NO^+ loss due to dissociative recombination is approximately equivalent to NO^+ production from charge exchange between O_2^+ and NO (reaction 5 of Table 2) and collisional rearrangement between O_2^+ and N (reaction 4) and O^+ and N_2 (reaction 11). At 1.5 sec, NO^+ becomes the major ion species with a concentration of $4 \times 10^6 cm^{-3}$.

---

20. Keneshea, T.J. (1967) A Technique for Solving the General Reaction Rate Equations in the Atmosphere AFCRL-67-0211, Environmental Research Papers No. 263.

21. Keneshea, T.J., Zimmerman, S.P., and Philbrick, C.R. (1976) A Dynamic Atmospheric Model, AFGL, Hanscom AFB, to be published.

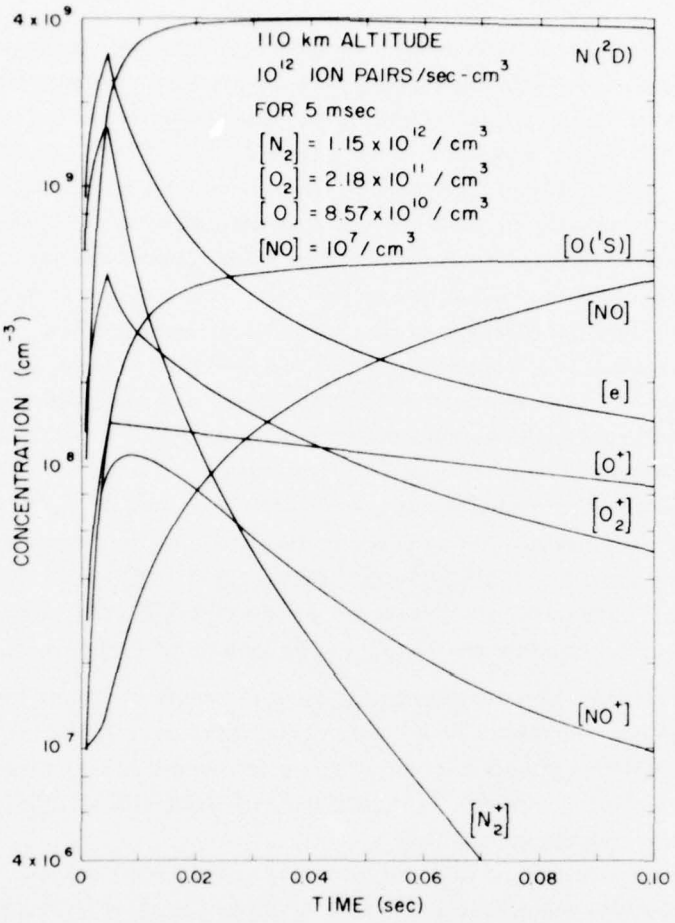

Figure 8a. Calculated Time Dependent Species Concentration Induced by EXCEDE II

(c) N(^{2}D) concentration peaks shortly (0.05 sec) after beam turn off and decays exponentially with the principal loss process, the reaction with O_2 forming vibrationally hot NO (reaction 14). At 100 km, the radiating fraction of N(^{2}D) represents only 10^{-5} of the total depopulation rate.

The bulk of N(^{2}D) forms vibrationally hot nitric oxide, NO, which in turn radiates at 2.7 and 5.4 μm. Investigation of the detailed band profiles, specific reaction mechanisms, and photon yields for NO and NO^+ infrared emissive processes is a primary scientific objective of this experiment.

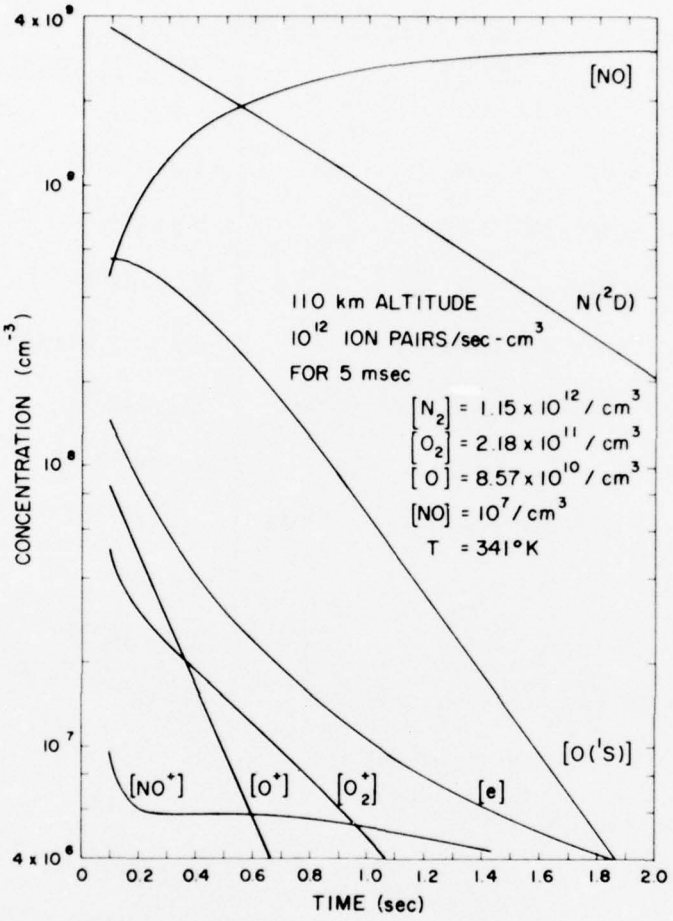

Figure 8b. Calculated Time Dependent Species Concentration Induced by EXCEDE II

Table 2. Shortwave Infrared Chemistry

Number	Reaction	Rate ($cm^3 sec^{-1}$)
1	$N_2^+ + O_2 \rightarrow N_2 + O_2^+$	5×10^{-11}
2	$N_2^+ + e \rightarrow N(^2D) + N(^4S)$	$1.8 \times 10^{-7} \times (300/T_e)^{0.39}$*
3	$O_2^+ + e \rightarrow 1.7\ O(^3P) + 0.27\ O(^1D) + 0.03\ O(^1S)$	$2.1 \times 10^{-7} \times (300/T_e)^{0.7}$

Table 2. (Continued)

Number	Reaction	Rate ($cm^3 sec^{-1}$)
4	$N + O_2^+ \rightarrow NO^+ + O$	1.8×10^{-10}
5	$O_2^+ + NO \rightarrow NO^+ + O_2$	4.4×10^{-10}
6	$N_2^+ + NO \rightarrow NO^+ + N_2$	3×10^{-10}
7	$O^+ + NO \rightarrow NO^+ + O$	1.3×10^{-12}
8	$NO^+ + e \rightarrow N(^2D) + O(^3P)$	$4 \times 10^{-7} \times (300/T_e)^{0.5}$
9	$O + N_2^+ \rightarrow NO^+ + N(^2D)/2 + N(^4S)/2$	2.5×10^{-10}
10	$O + N_2^+ \rightarrow N_2 + O^+$	1×10^{-12}
11	$N_2 + O^+ \rightarrow NO^+ + N(^2D)/2 + N(^4S)/2$	1×10^{-12}
12	$O_2 + O^+ \rightarrow O + O_2^+$	2×10^{-11}
13	$N + NO \rightarrow N_2 + O$	2.5×10^{-11}
14	$N(^2D) + O_2 \rightarrow NO + O$	6×10^{-12}
15	$N_2 + e \rightarrow N(^2D)/2 + N(^4S)/2 + N^+ + 2e$	†
16	$N_2^+ + N \rightarrow N_2 + N^+$	1×10^{-11}
17	$N^+ + O \rightarrow N + O^+$	1.2×10^{-12}
18	$N^+ + O_2 \rightarrow N + O_2^+$	3×10^{-10}
19	$N^+ + O_2 \rightarrow NO^+ + O(^1S)$	3×10^{-10}
20	$N^+ + O_2 \rightarrow O^+ + NO$	1×10^{-12}
21	$N^+ + NO \rightarrow N + NO^+$	8×10^{-10}
22	$N^+ + NO \rightarrow N_2^+ + O$	3×10^{-12}
23	$N^+ + NO \rightarrow O^+ + N_2$	1×10^{-12}
24	$N(^2D) + N_2 \rightarrow N(^4S) + N_2$	1.6×10^{-14}
25	$N(^2D) + NO \rightarrow N(^4S) + NO$	7×10^{-11}

Table 2. (Continued)

Number	Reaction	Rate ($cm^3 sec^{-1}$)
26	$N_2(A) + NO \rightarrow NO(A) + N_2$	7.0×10^{-11}
27	$N_2(A) + O_2 \rightarrow N_2 + O_2$	4.0×10^{-12}
28	$N_2(A) + O(^3P) \rightarrow N_2 + O(^1S)$	3.0×10^{-11}
29	$N_2(A) + N \rightarrow N_2 + N$	5.0×10^{-11}
30	$N_2 + NO^{(\ddagger)} \rightarrow N_2^{(\ddagger)} + NO + (h\nu)$	4.0×10^{-17}
31	$N(^4S) + O_2 \rightarrow NO^{(\ddagger)} + O$	1.0×10^{-16}
32	$N + N + M \rightarrow N_2 + M$	$\left(5 \times 10^{-33} (I/300)^2\right)^{**}$
33	$O_2 + NO^{(\ddagger)} \rightarrow O_2^{(\ddagger)} + NO + (h\nu)$	1.0×10^{-14}

*T_e represents electron temperatures in (°K).

†Twenty-five percent of the ion pairs produced by electron impact on nitrogen are assumed the result of reaction 15. Ion-pair production in the range of 10^7 to 10^{14} ion pairs cm^{-3} sec^{-1} is treated as an initial condition.

**The units of this three-body reaction are $cm^6 sec^{-1}$.

9. NO AND NO^+ RADIANCE LEVELS

The 13 April 1975 EXCEDE II test rocket launch provided measurements of electron-induced photometric and radiometric quantities at 110 km as summarized in Table 3. As previously discussed, the payload-based photometric and radiometric data are a measure of the near field volume emission rate as determined by the electron deposition geometry, payload velocity, and the characteristic production and/or emission time constant. The results in Table 3 show a 5577 to 3914Å photon emission ratio of 2.9×10^{-2} at 110 km in contrast to steady state values measured in aurora in the range of 0.4 to 4 with 2 a representative nominal value.[19]

The data may be interpreted in terms of basic aeronomic mechanisms by estimating total band intensity, characteristic production/emission time constants, and the principal production processes. In Figure 9 is presented calculated time-dependent volume emission rates for a number of radiating species using the reaction set of Table 2 and the mathematical technique and experimental conditions similar to those assumed to produce Figure 8. The dosing magnitude, dosing duration, and ambient atmospheric densities are those considered representative of the proposed experiment at 110 km. The

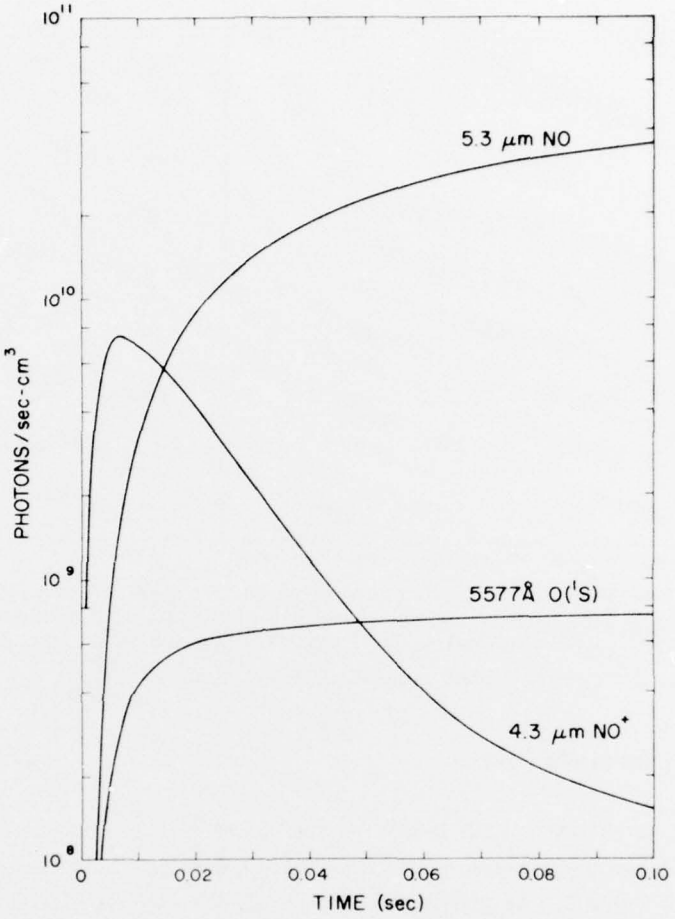

Figure 9a. Calculated Time Dependent Volume Emission Rates for the Proposed EXCEDE II Experiment at 110 km

Table 3. EXCEDE II: Test Photometric and Radiometric Data

(Altitude 110 km, Beam 3 kV, 5A)

Filter Wavelength	Filter Bandwidth	Measured Radiance
3916Å	18.5Å	34. MR*
5582Å	9.2Å	1.3 MR
2.626 μm	0.637 μm	44. MR
4.277 μm	0.089 μm	3.4 MR

*Megarayleighs (10^{12} photons $cm^{-2}sec^{-1}$) as measured by payload based sensors on the 13 April 1975 launch.

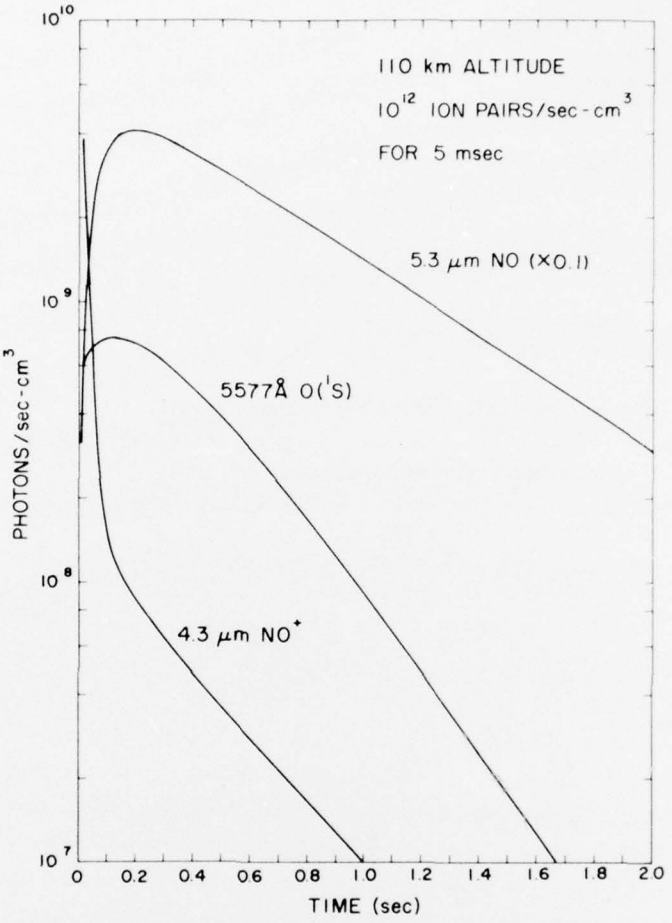

Figure 9b. Calculated Time Dependent Volume Emission Rates for the Proposed EXCEDE II Experiment at 110 km

results presented in Figure 9 additionally assume that 10 infrared photons are produced from each NO molecule formed in reaction 14 and all reactions forming NO^+ yield one infrared photon. The model calculations of Figure 9 indicate the $O(^1S)$ emission profile has a slightly faster rise and decay time than the NO infrared emission. Thus, as viewed from a moving payload, the faster production and/or emission time constant of 5577Å emission is viewed more effectively than the NO infrared chemiluminescence. Table 4 has been generated from Table 3 and is presented as preliminary results subject to revision when a

Table 4. EXCEDE II Test: Steady State Intensity Estimate

Emitter	Integrated Intensity[1] (Megarayleighs)	Characteristic Time Constant[2] (Sec)	Steady State Radiance[3] (Megarayleighs)	Luminous Efficiency[4]
N_2^+ 3914 A	45.	7×10^{-8}	45	4×10^{-3}
$O(^1S)$ 5577A	1.3	0.74	90	5.6×10^{-3}
NO 2.7 μm	44.	0.76	3000	4×10^{-2}
NO^+ 4.3 μm	10.	3×10^{-3}		
CO_2 4.3 μm		10^{+4}		

1. The integrated intensity is based on the measurements of Table 3, the interference-filter optical bandwidths, and an estimated band profile.
2. Time is the estimated characteristic emission time constant as limited by either production or loss processes.
3. The steady state radiance is estimated assuming the 5577/3914Å ratio is 2, normalized to 45 MR of 3914Å emission.
4. The electron induced luminous efficiency is based on a value of 4×10^{-3} for N_2^+ 3914Å emission as reported by O'Neil et al.,[13] in the PRECEDE experiment.

more rigorous analysis includes effects of payload aspect, electron-beam pitch angle and photometric and radiometric radiance values for a wide range of altitudes. In Table 4 it is indicated that the estimated characteristic production emission times for both $O(^1S)$ and NO infrared radiation are similar at 110 km, providing a convenient scaling factor to convert the observed emissions into steady state values. The scaling factor to estimate the 4.3-μm steady state radiant intensity in Table 4 is uncertain until the emitting specie(s) and the production processes are more clearly delineated. The electron-induced radiant efficiency, as presented in Table 4, is the fraction of the electron-beam energy emitted in a given molecular or atomic transition as the primary electron and all secondaries are stopped in the atmosphere. The radiant efficiency of 4×10^{-2} for NO 2.7-μm emission given in Table 4 is considered a preliminary value based on an assumed production process, rate coefficient, and molecular band profile. The integrated photon yield of the NO fundamental emission at 5.4 μm has been calculated[22] to be approximately 5 times the 2.7 μm overtone photon yield for the case where the vibrational levels 1 through 17 are populated in direct proportion to their vibrational level, and vibrational relaxation proceeds according to the

22. Rogers, J.W. (1976) OPR, AFGL, Hanscom AFB, Private communication.

transition probabilities of Cashion.[23] This calculated fundamental to overtone photon yield suggests an electron-induced radiant efficiency of 0.1 for NO emission at 5.4μm. Thus an estimated 14 percent (considered a lower limit) of the primary electron energy is radiated in NO emission at 2.7 and 5.4μm as the electron is stopped in the atmosphere. It is stressed that the radiant efficiency inferred for the NO infrared emission at 2.7μm in Table 4 is a preliminary value based on a series of assumptions required to convert the payload-based photometric and radiometric measurements to steady state photon emission rates. A complete treatment of the data from both the EXCEDE II test launch and the EXCEDE:SWIR experiment will provide a wide range of experimental conditions on which to test the various assumptions and to base a more definitive result.

10. PAYLOAD INSTRUMENTATION

The principal payload-based sensors are a series of optical and infrared instruments coaligned in the instrument bay shown in Figure 6. In the proposed experiment, the optical sensors are coaligned with similar fields of view and densely packaged to minimize differences in aspect with which the sensors observe the electron excited atmosphere. The scientific approach is to monitor a number of optical emissions with reasonably well-established mechanisms for production, radiation, and collisional depopulation as diagnostics of the electron energy dosing magnitude and photon yields. Less certain infrared chemical processes and photon yields are defined relative to the optical diagnostic emissions such as N_2^+ 1N 3914Å and $O(^1S)$ 5577Å radiation, which are also measured by the ground-based telephotometer. Optical and infrared emissions of specific interest, their measurement objective, and the estimated radiance magnitude as observed by payload-based sensors at 110 km are given in Table 5. The radiance values in Table 5 are in part based on the EXCEDE II test measurements normalized to the N_2^+ 1N 3914Å radiance anticipated in the proposed experiment with the assumption the four electron-gun cathodes are separated from the optical and infrared sensors by 40, 70, 100, and 130 cm. Table 5 also indicates the spectroscopic features measured by the ground-based instruments. The ground-based photometric measurements integrate over the total atmospheric volume excited by the electron accelerator and provide an essential supplement to the payload measurements which are significantly weighted toward the prompt emissions as indicated by the 5577Å/3914Å photon emission ratio measured in the EXCEDE II test launch

23. Cashion, J.K. (1963) Calculating vibrational transition probabilities, J. Mol. Spectrosc. **10**:182.

Table 5. EXCEDE II: Estimated Radiance for Payload Based Sensors (Payload Altitude 110 km)

Wavelength	Radiating Specie	Payload Based Radiance*	Significance	Payload Based Sensors				Ground Based Sensors	
				Spectro-meter	Photo-meter	Interfero-meter	Radio-meter	Spectro-graph	Telephoto-meter
2890 Å	CO_2^+	40 KR	CO_2 density	x	x				
3433 Å	N_2VK(1-10)	16 KR	N_2A state	x					
3466 Å	N(^{2}P)	0.9 KR	NO precursor	x	x				
3914 Å	N_2^+ 1N(0-0)	140 MR	Beam diagnostic	x	x				x
4057 Å	N_2 2P(0-3)	6 MR	Secondary electron diagnostic	x					
4416 Å	O II	320 KR	O density	x				x	
5062 Å	$N_2$2P(3-10)	82 KR	Dynamic range control	x				x	
5140 Å	N_2^+ 1N(1-4)	530 KR	Dynamic range control	x				x	
5198 Å	N(^{2}D)	0.3 KR	NO precursor	x	x				
5270 Å	O_2^+ 1N(2-0)	10 MR	O_2 density O_2 production	x				x	
5577 Å	O (^{1}S)	4 MR	Slow emission monitor	x	x			x	x
2.7 μm	NO	270 MR	NO overtone			x	x		
4.3 μm	NO^+, CO_2	30 MR	NO^+ fundamental			x	x		
5.4 μm	NO	1,400 MR	NO fundamental			x	x		

*Payload-based radiance for selected emissions within the bandwidths of the spectral instruments.

(Table 3). The length of time the ground based optical sensors observe the decay of electron-induced atmospheric emissions is determined by the payload trajectory, the sensor field of view, and the sensor viewing aspect. Afterglow "look times" are typically in the range of 1 to 30 sec for the ground-based optical systems. The principal payload instruments are listed in Table 6. The primary diagnostic instrument for this experiment is the short-wave infrared interferometer using liquid-nitrogen cooled optics to suppress the limitation of minimal detectable radiance introduced by thermal radiation from the instrument. In the payload orientation shown in Figure 6, thermal radiation from the lower atmosphere and the earth's surface is a 45-deg off-axis source and is attenuated below the detectability threshold by the instrument design. Design specifications for the interferometer are given in Table 7.

Table 6. EXCEDE II: Payload Instruments

Instrument	Size (in.)	Weight (lb)
Electron accelerators (4 modules)	12 x 32 each 48 x 32 total	480 each 1920 total
Liquid N_2 interferometer	10 x 28	60
LN_2 CVF spectrometer	6 x 16	25
LN_2 radiometer	6 x 16	25
LHe CVF spectrometer	10 x 24	75
UV/visible spectrometer	10 x 24	75
Photometers (5 units)	7 x 2 x 1.25 each 7 x 2 x 6.25 total	1 each 5 total
Camera*		
Diagnostics* RPA impedance probe		
Magnetometer*		
		2185

*The size and weight of these instruments are not defined and/or do not significantly contribute to the total payload size and weight.

Table 7. SWIR Interferometer Specifications

Spectral Range	2.0 to 5.6 μm
Resolution	2 cm^{-1}
Field-of-View	2.29°; 1.26 × 10^{-3} sr
Scan Time	2.0 sec total 0.2 sec retrace 1.8 scan period
NESR*	7 × 10^{-11} W $cm^{-2}sr^{-1}cm$
Dimensions	10.5 × 29.3 in.

*Noise Equivalent Spectral Radiance at 2μm, estimated value.

The electron-beam pulse format and the interferometer scan period are shown in Figure 10. It is proposed that the electron accelerator be pulsed for 4 sec followed by a 2-sec off period, a sequence repeated in an 18-sec pulse frame for the duration of the experiment. In the initial 12 sec of the 18-sec pulse frame, the four-electron-gun modules are synchronously pulsed for 4 sec providing a total current of 40 A. The third pulse in each frame is provided by a single module, gun 1 of Figure 6, producing a 10-A beam. This pulse format represents a 50-percent duty factor for the 120-kW electron accelerator. As configured in Figure 6, gun 1 with minimal cathode sensor separation provides approximately 40 percent of the total radiance produced by a full-power accelerator pulse as observed by the payload sensors. Observation of the relative radiance of various emissions with beam current provides a measure of the time dependent emission rate as a function of dosing magnitude. This information, in turn, provides insight into the basic aeronomic production and loss processes. At the initiation of each 4-sec electron-beam pulse a synchronous reset pulse activates the interferometer retrace drive which positions the movable mirror at the start position. The interferometer initiates a scan approximately 0.2 sec after the reset pulse. During this 0.2-sec period the movable mirror is reset in the start position from any place within its operating limits and the electron-beam induced atmospheric emissions establish an apparent steady state intensity as viewed from the payload. The apparent steady state intensities are controlled by the beam geometry, payload trajectory, and sensor orientation where the bulk of the integrated column radiance comes from the first few meters near the payload, as shown in Figure 7 for the case of prompt emissions. As viewed by the

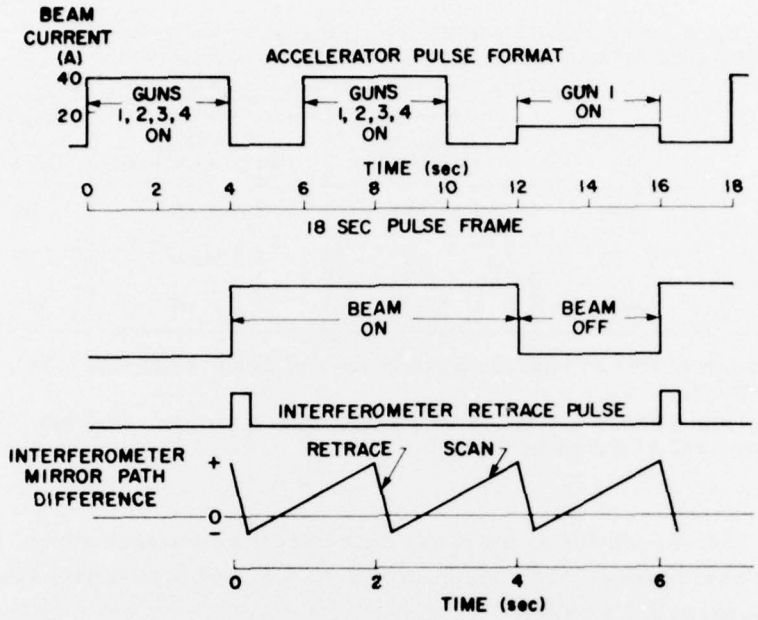

Figure 10. Accelerator Pulse Format and Interferometer Scan Rate

payload-based sensors, the electron-beam induced optical and infrared emissions are anticipated to establish an essentially constant value in a period much less than 0.2 sec. As shown in Figure 10, the interferometer completes 2 cycles during the beam-on period and 1 cycle during the off period. The electron beam-on and -off periods are made nearly integer multiples of the interferometer period. After the reset pulse initiates interferometer retrace at the start of each electron-beam pulse, the interferometer continues to sweep completing 3 cycles during the 6-sec beam pulse period. The beam-off transition period where the accelerator-induced emissions decay to an ambient atmospheric level coincides with a 0.2-sec interferometer retrace. In order to readily interpret the interferograms, it is required that the relative spectral radiance of the observed emissions be stable during an interferometer scan. This requirement is satisfied for the proposed experiment for the payload orientation shown in Figure 6 and the pulsing format shown in Figure 10. As configured, the interferometer is anticipated to observe infrared emissions which rapidly attain a quasi-steady state radiance magnitude and show gradual changes in intensity with atmospheric density.

Table 8. Estimated Interferometer Signal to Noise Ratios
(Payload altitude 110 km: 120 kW electron accelerator)

Emission (μm)	Intensity (MR)	Average Intensity* (MR μm^{-1})	Average Intensity ($Wcm^{-2}sr^{-1}cm$)	Signal to Noise Ratio**
2.7	270	585	2.5×10^{-9}	50
4.3	30	120	8.1×10^{-10}	20
5.3	1,400	2,400	2.0×10^{-8}	500

*Average intensities are based on the results of Table 5 and estimated band profiles.

**Signal to noise ratios are based on a single interferometer scan for the instrument specified in Table 7.

As indicated by Table 8, the short-wave infrared interferometer is anticipated to readily record the emissions at 2.7, 4.3, and 5.4 μm with substantial signal to noise ratios.

A number of photometric and radiometric sensors included in Table 6 monitor the time-dependent radiance magnitude of several emissions to assess the source stability during an interferometer scan and to assist in establishing absolute radiance magnitudes. A circular variable filter (CVF) infrared spectrometer is included as a low-resolution instrument in the 2.0- to 5.6-μm range supplemental to the interferometer. The ultraviolet/visible spectrometer monitors a number of emissions providing diagnostics of the electron-beam dosing magnitude. The ultraviolet and optical emissions indicated in Table 5 also include a number of emissions, $N(^2D)$ and $N(^2P)$, considered precursor species to the NO infrared chemiluminescence. Other emissions included in Table 5 provide a monitor of ambient atmospheric conditions of relative species concentration (N_2, O_2, O, and CO_2) and kinetic temperature.

Two cameras, located in the instrument bay, are proposed to document the electron-beam deposition geometry and the viewing aspect of the optical and infrared sensors relative to the primary electron deposition region. The two cameras consist of a narrow, approximately 10 deg, and wide angle, 100 deg, field of view system coaligned with the optical and infrared sensors. With the radiance magnitudes indicated in Table 5, commercially available films with f/2 lenses would record meaningful image densities with exposures on the order of a few milliseconds.[24] An exposure sequence based on preflight estimates of

24. Kofsky, I. L. and Sluder, R. B. (1976) Photometrics, Inc., Lexington, Mass., Private communication.

source radiance and selected to record a wide dynamic range of radiance would be controlled in flight by an intervalometer. The cameras record the near-field electron-beam deposition geometry and the optical sensor viewing direction. This information is required in the interpretation of absolute radiances measured by the photometers and radiometers with given optical alignments. The photographic systems obviously assume successful recovery of the instrument bay.

II. GROUND-BASED OPTICAL SYSTEMS

In previous launches in the EXCEDE program ground-based optical systems included film and television cameras, a two-color telephotometer system, and an image intensified spectrograph. In Figures 3 and 4 results from ground-based cameras used in the PRECEDE launch are given.

Spectra of optical emissions induced by the PRECEDE electron accelerator were obtained using a ground-based objective mode image-intensified spectrograph with film recording. This instrument, designed, fabricated, and operated in the field by HSS, Inc., was designated the Cygnus spectrograph. Precision radar controlled tracking by WSMR allowed long exposure times without introducing image motion smearing. Optical wavelength coverage extended from 4200 Å to 8500 Å and the spectral resolution was 10 Å. A 2-sec exposure of the image intensified spectrograph is shown in Figure 11 for a payload altitude of 92 km during the descent trajectory. The absolute radiometric scale of the data is based on laboratory calibration with an irradiance standard. Corrections were made for atmospheric attenuation by Rayleigh and aerosol scattering but not molecular band absorption.

The prominent molecular features of the spectra are the 4278 Å (0-1) and 4709 Å (0-2) bands of the N_2^+ 1N system, 13 bands of the $\Delta v=1$, 2, and 3 sequences of the N_2 1 P system, and 5 bands of the $\Delta v=2$ and 3 sequences of N_2^+ Meinel system. The N_2^+ Meinel and the N_2 1P systems show the effects of collisional deactivation in the 80- to 110-km altitude range.

The 5577A $O(^1S)$ afterglow produced a tail in the spectrographs extending from the otherwise point image spectra. Spatial scans along this tail showed the exponential decay of this forbidden line over a 1-sec interval. Measured decay times include: 0.61 sec at 113 km, 0.49 at 103 km, and 0.25 at 89 km, in general agreement with the telephotometer results.

The PRECEDE experiment included a ground-based two-channel telephotometer measurement of the time-dependent emission rate of N_2^+ 1N 3914Å and $O(^1S)$ 5577 Å radiation induced in the night atmosphere by the rocketborne 2-kW electron accelerator (Figure 12). The telephotometer shared a common tracking

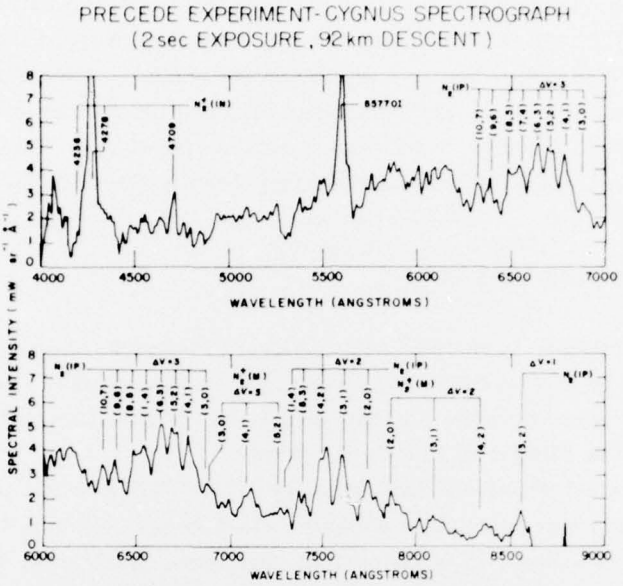

Figure 11. Results from the Image Intensified Spectrograph Designed, Fabricated, and Operated by HSS, Inc. of Bedford, Mass.

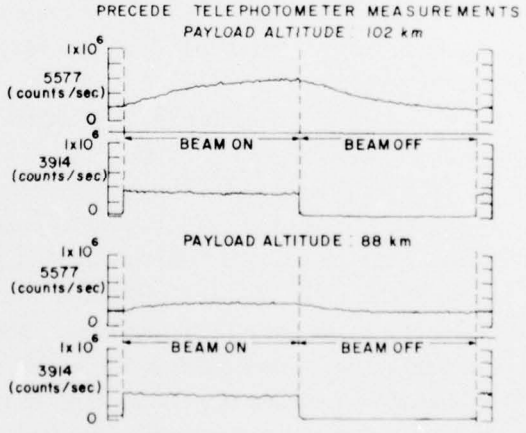

Figure 12. Telephotometer Measurement of the N_2^+ 3914 Å and $O(^1S)$ 5577 Å Time Dependent Emission Induced at 102 and 88 km by the 2-kW Electron Accelerator, Square Wave Modulated at 0.5 Hz. The effects of collisional deactivation are apparent in the reduced emission of $O(^1S)$ at the lower altitude

mount with the image-intensified sepctrograph arranged to view the dosed atmosphere such that it presented a minimal apparent source size. Photon count rates in the range of 1 to 8 x 10^5 counts per sec were recorded for the 3914- and 5577-Å emissions. Monitors of the electron accelerator power have been combined with telephotometer calibration to determine the radiant efficiency for N_2^+ 1N 3914Å production by 2.5-kV electrons in the 80- to 120-km altitude range. Several stars providing count rates comparable to the electron source and of similar azimuth and elevation were monitored to calibrate the system absolutely, including the effects of atmospheric extinction. A preliminary value of 4.2 x 10^{-3} is given for 3914Å electron induced luminous efficiency in the altitude range 80 to 120 km. The time dependent 5577 O(^{1}S) emission data has been analyzed in terms of production and loss processes. At altitudes near apogee (120 km) it is apparent O(^{1}S) emission is produced by consecutive reactions with the reaction of N_2(A) and O the primary production process. At lower altitudes other processes become increasingly important.

Super Cygnus, an improved version of the Cygnus spectrograph, has been designed and fabrication has been initiated. Specifications for both spectrographs are compared in Table 9. The spectra shown in Figure 11 represent a 2-sec exposure of a 2-kW electron accelerator. Effective deployment of the Super Cygnus spectrograph in support of the 120-kW electron accelerator potentially represents an increase of a factor of 900 in the film exposure rate over the Cygnus spectrograph results for atomic emissions in the PRECEDE experiment. The increased measurement capability is due to the combined effects of accelerator

Table 9. Image-Intensified Ground-Based Spectrographs

Parameter	Cygnus	Super Cygnus
Wavelength range	4200 to 8500 Å	4200 to 7500 Å
Resolution	10 Å	1 Å
Relative aperture	f/1.5	f/1.5
Field of view (variable)	0.5 to 2.0 deg	0.5 to 2.0 deg
Image intensifier radiant power gain	40,000	40,000
Film format	70 mm	70 mm
Exposure times (optional)	1, 2, 5, 10, 20 sec	1, 2, 5, 10, 20 sec
Relative system sensitivity	1	15

power and relative system sensitivity. The potential increase in system performance provides an opportunity to precisely monitor the altitude dependence of all the atomic and molecular features indicated in Figure 11 as well as a large number of less prominent atmospheric emissions. A calculation based on estimated performance characteristics of the EXCEDE II accelerator and Super Cygnus indicates that the $N(^2D)$ doublet at 5198.5 and 5200.7 Å is resolved and provides count rates at the image intensifier photocathode on the order of several hundred photoelectrons per resolution element in a 4-sec exposure. The calculation assumes a payload altitude of 110 km and the cylindrical 120-kW electron source is viewed with a 10 to 1 aspect ratio. The intensified spectrograph, anticipated to be source photon noise limited, provides a ground-based measure of the $N(^2D)$ emission with an uncertainty of 10 percent or less for the case considered. A ground-based measurement of the $N(^2D)$ altitude emission profile provides an independent measurement of this specie (considered the precursor source of vibrationally hot nitric oxide) to support the payload-based infrared measurements.

12. CONCLUSIONS

The proposed EXCEDE II experiment studies the detailed band profiles of the short-wave infrared emissions induced in the 80- to 120-km altitude range by a rocketborne 120-kW electron accelerator. The experiment is an extension of the technique successfully used in the three initial launches in the EXCEDE program. The estimated radiance of the infrared emissions is anticipated to be readily measured by both the interferometer and the circular variable filter spectrometer. Emphasis in the proposed experiment is the spectral measurement of ultraviolet, optical, and infrared electron-induced emissions rather than the photometric and radiometric measurements used in the initial experiments. Advantages inherent in the spectral measurements include the unambiguous identification of the radiating species, the precise measurement of relative radiances by a common detection system, and the measurement of detailed molecular band profiles. The magnitude of the atmospheric emissions, the capability of ground support systems, and the engineering design of the proposed experiment are extensions of the technological base established in the earlier EXCEDE launches.

References

1. Rees, M.H. and Jones, R.A. (1973) Time dependent studies of the aurora—II. Spectroscopic morphology, Planet. Space Sci. **21**:1213.

2. Judge, R.J.R. (1972) Electron excitation and auroral emission parameters, Planet. Space Sci. **20**:2081.

3. Banks, P.M., Chappell, E.R., and Nagy, A.F. (1974) A new model for interaction of auroral electrons with the atmosphere: Spectral degradation, backscatter, optical emission, and ionization, J. Geophys. Res. **79** (No. 10):1459.

4. Rees, M.H. and Luckey, D. (1974) Auroral electron energy derived from ratio of spectroscopic emissions: 1. Model computations, J. Geophys. Res. **79** (No. 34):5181.

5. Slanger, T.G. and Black, G. (1973) $O(^1S)$ quenching profile between 75 and 115 km, Planet. Space Sci. **21**:1757.

6. O'Neil, R.R., Lee, E.T.P., Huppi, E.R., and Stair, A.T. (1973) Project EXCEDE:SWIR Experiment, AFCRL-TR-73-0152, Environmental research papers, No. 437.

7. Berger, M.J., Seltzer, S.M., and Maeda, K. (1970) Energy deposition by auroral electrons in the atmosphere, J. Atmos. and Terr. Phys. **32** (No. 6):1015.

8. Berger, M.J., Seltzer, S.M., and Maeda, K. (1974) Some new results on electron transport in the atmosphere, J. Atmos. and Terr. Phys. **36**:591.

9. Hess, W.N., Trichel, M.C., Davis, T.N., Beggs, W.C., Kraft, G.E., Stassinopoulos, E., and Maier, E.J.R. (1971) Artificial aurora experiment: Experiment and principal results, J. Geophys. Res. **76** (No. 25):6067.

10. Shepherd, O., Carpenter, J.W., Reidy, W.P., Sheehan, W.A., and Zehnpfeunig, T.F. (1975) The Design and Flight Test of a 30 kw Rocket-Borne Electron Accelerator Module (EXCEDE II Test) HAES Report No. 22, AFCRL-TR-75-0379.

11. O'Neil, R.R., Stair, A.T., Jr., Ulwick, J.C., Burt, D., and Narcisi, R. (1976) EXCEDE: SWIR experiment, Quick Look Data Report.

12. Bien, F. and Baum, H.R. (1974) Detailed Investigation of Transient Electron Beam Deposition into the Atmosphere, Aerodyne Research, Inc., Report ARI-RR-50, Contract No. F19628-73-C-0048, Subcontract No. PO43081.

13. O'Neil, R.R., Huppi, E.R., and Lee, E.T.P. (1975) PRECEDE experiment: Ground based telephotometer measurements of N_2^+ 1N 3914Å and O(^{1}S) 5577Å emission (abstract), EOS Trans. AGU 56 (No. 12):1035.

14. Sandock, J.A., Burt, D.A. and Bien, F. (1975) PRECEDE experiment (abstract), EOS Trans. AGU 56 (No. 12):1035.

15. Bien, F., Baum, H. and Tait, K. (1975) An analysis of transient vehicle charging in the EXCEDE experiment (abstract), EOS Trans. AGU, 56 (No. 12):1035.

16. Cambou, F., Dokoukine, V.S., Ivchenko, V.N., Managadze, G.G., Migulin, V.V., Nazarenko, O.K., Nesmyanovitch, A.T., Pyatsi, A.KH., Sagdeev, R.Z., and Zhulin, I.A. (1975) The Zarmitza rocket experiment of electron injection, to be published in Space Research XV and Life Time Sciences XIII.

17. Cambou, F., Sagdeev, R.Z., Zhulin, I.A., Charles, G., and Dokoukme, V.S. (1976) General description of the ARAKS experiments (abstract), Program and Abstracts for the Symposium on Active Experiments in Space Plasmas, COSPAR, URSI, and IAGA, June 3-5, 1976, Boulder, Colo.

18. Reme, H., Saint-Marc, A., Vigo, J.M., Gringauz, K.I., Managadze, G.C., Lyakhov, S.B., Smirnova, L.P., Schutte, N.M., and Sheldon, W.R. (1976) Results of the ARAKS particle experiments (abstract), Program and Abstracts for the Symposium on Active Experiments in Space Plasmas, COSPAR, URSI, and IAGA; June 3-5, 1976, Boulder, Colo.

19. Vallance-Jones, A. (1971) Auroral spectroscopy Space Sci. Reviews 11:776.

20. Keneshea, T.J. (1967) A Technique for Solving the General Reaction Rate Equations in the Atmosphere AFCRL-67-0211, Environmental Research Papers No. 263.

21. Keneshea, T.J., Zimmerman, S.P., and Philbrick, C.R. (1976) A Dynamic Atmospheric Model, AFGL, Hanscom AFB, to be published.

22. Rogers, J.W. (1976) OPR, AFGL, Hanscom AFB, Private communication.

23. Cashion, J.K. (1963) Calculating vibrational transition probabilities, J. Mol. Spectrosc. 10:182.

24. Kofsky, I.L. and Sluder, R.B. (1976) Photometrics, Inc., Lexington, Mass., Private communication.